

Unique Monotropic Phase Transition Behaviors of a Butterfly-Shaped Diphenylpyrimidine Molecule

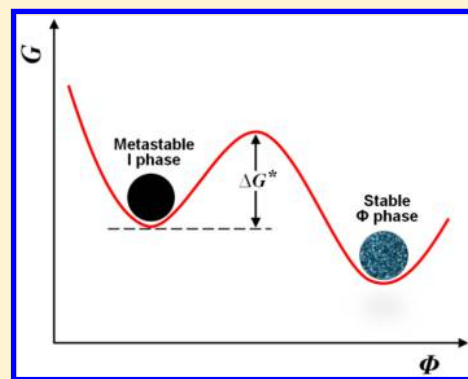
Minwook Park,[†] Yu-Jin Choi,[†] Dae-Yoon Kim,[†] Seok-Ho Hwang,^{*,‡} and Kwang-Un Jeong^{*,†}

[†]Polymer Materials Fusion Research Center & Department of Polymer-Nano Science and Technology, Chonbuk National University, Jeonju 561-756, Korea

[‡]Department of Polymer Science and Engineering, Dankook University, Yongin, Gyeonggi 448-701, Korea

S Supporting Information

ABSTRACT: The physical properties of two-dimensional disc-shaped aromatic carbon molecules strongly depend on the molecular packing structures. A butterfly-shaped diphenylpyrimidine molecule (DPP-6C12) was synthesized by covalently attaching two tridodecyl benzoate tails (6C12) at the both sides of the diphenylpyrimidine (DPP) moiety. Unique phase transition behaviors of DPP-6C12 and their origins were investigated with the combined techniques of thermal, scattering, spectroscopic, and microscopic analyses. On the basis of the experimental results and analyses, it was realized that a butterfly-shaped DPP-6C12 formed three ordered phases: a plastic crystal phase (PK), a crystal phase (K), and a liquid crystal phase (Φ). By breaking the molecular symmetry and coplanarity of DPP-6C12, peculiar monotropic phase transition behaviors were observed. The stable Φ mesophase was formed either by a slow heating above the metastable PK phase or by an isothermal annealing between T_{Φ} and T_K . The stable K phase was only formed by a slow heating from the preordered Φ mesophase, and the formation of the K phase directly from the isotropic state (I) was forbidden because the nucleation barrier from I to K was too high to be overcome via thermal annealing.



INTRODUCTION

The phase transition behavior of soft materials is an interesting phenomenon when more than one ordered phase exists.¹ Especially, liquid crystalline (LC) soft materials show the enantiotropic LC transition behaviors with the thermodynamic stability in a temperature region between their melting and isotropic (I) temperatures. Monotropic LC soft materials, on the other hand, show metastable states when the crystallization is bypassed below the LC transition temperature with a fast cooling rate. Therefore, the formation of the monotropic state is usually originated from the competition between the crystal phase and the LC phase.^{2–8} This type of phase transition allows us to study the formation of crystals either from the I melt or from the LC phase.^{9–12} Additionally, since the physical properties of LC soft materials strongly depend on molecular self-assembly, it is essential to control their molecular packing structure on the different length scales and times from subnanometer to micrometer.¹³

The molecular interactions between disc-shaped aromatic mesogens can be tuned by attaching flexible alkyl or alkoxy groups at the periphery of the rigid core with chemical or physical bonds. The traditional disc-shaped LC mesophases can be constructed by adjusting the thermal energy in the system.¹³ Upon decreasing the temperature below the I phase, the aspect ratios of the self-assembled nanocolumns are suddenly increased. Here, the formation of nanocolumns is mainly driven by the strong π – π interactions between disc-shaped

aromatic cores and the nanophase separation between the rigid disc-shaped core and flexible alkyl or alkoxy tails.¹⁴ Furthermore, the self-assembled nanocolumns can laterally organize each other and show one- or two-dimensional (1D or 2D) long-range molecular orientational or positional orders. In this partially ordered thermotropic mesophase, the flexible alkyl or alkoxy tails remain in the disordered state. When the temperature is further decreased, the flexible tails even crystallize in the phase-separated nanodomains and the highly ordered columnar crystalline phase is formed.¹⁵

Usually, the existence of the low-ordered LC mesophase is favorable for practical application of the disc-shaped molecules since the macroscopic molecular orientation even on the meter length scale can be achieved by applying mechanical, electrical, or magnetic forces with the support of surface anchoring and confinement. In organic photovoltaic (OPV) device and organic thin film transistor (OTFT) applications of disc-shaped molecules,^{16–19} the strong π – π interactions between the rigid cores are favorable to improve the physical device performance, since the electrical, thermal, and photoconductivity along the columnar long axis is significantly increased by the π – π strong interactions between the rigid cores. However, in the organic light emitting diode (OLED) application,^{20–22} device engineers

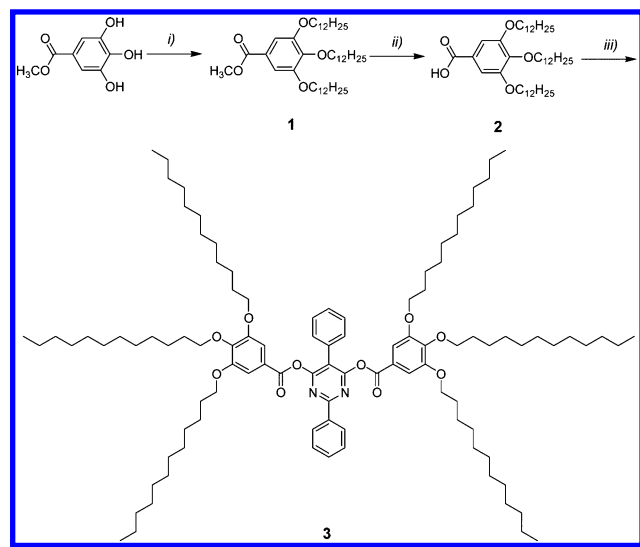
Received: November 21, 2014

Revised: January 7, 2015

and physicists would like to avoid molecular packings since the strong π - π interactions between the rigid cores generate excimers which may decrease the photoefficiency of the system.²³

To understand the self-assembly process of a LC molecule with the broken symmetry and the low coplanarity, a diphenylpyrimidine-based molecule (abbreviated as DPP-6C12, Scheme 1) was newly designed and synthesized by

Scheme 1. Reagent and Conditions: (i) K_2CO_3 , 1-Chlorododecane, DMF, Reflux; (ii) KOH, Ethanol, Reflux; (iii) (1) $SOCl_2$, THF, (2) NaH, THF, Reflux



chemically attaching two tridodecyl benzoate tails (6C12) at the both sides of the diphenylpyrimidine (DPP) moiety via three-step reactions.^{24–26} Here, 6 and 12 represent the numbers of alkyl tails of DPP-6C12 and carbon atoms in each alkyl tail, respectively. Major phase transitions of DPP-6C12 and their origins were systematically investigated by the combined techniques of differential scanning calorimetry (DSC), 1D wide-angle X-ray diffraction (WAXD), polarized optical microscopy (POM), and solid-state carbon-13 (¹³C) nuclear magnetic resonance (NMR) spectroscopy.

EXPERIMENTAL SECTION

The general procedures of chemical treatments and characterizations were described in the Supporting Information. Additionally, the experimental conditions and sample preparation procedures of DSC, 1D WAXD, POM, MALDI-ToF, and solid-state ¹³C NMR are explained in detail in the Supporting Information.

Methyl 3,4,5-Tris(*n*-dodecan-1-yloxy)benzoate (1). After K_2CO_3 (44.5 g, 330 mmol) was added into the solution of methyl 3,4,5-trihydroxybenzoate (10 g, 54 mmol) in DMF (100 mL), 1-chlorododecane (51.2 mL, 217 mmol) was then slowly introduced. The mixture was additionally stirred for 12 h at 100 °C. The gummy solid obtained by filtration and evaporation was dissolved in chloroform. The resulting mixture was washed with brine and deionized water (50 mL \times 3) and dried over anhydrous Mg_2SO_4 and then filtrated. The crude product was purified by column chromatography (SiO_2) with a mixture of dichloromethane and hexane (4:1, v/v), followed by recrystallization from acetone to give a white solid (28.3 g, 76%): ¹H NMR (400 MHz, $CDCl_3$, δ): 7.24 (s, 2H; CH), 4.00 (m, 6H; CH_2), 3.88 (s, 3H; CH_3), 1.81–1.77 (m, 6H; CH_2), 1.45–1.24 (m, 54H; CH_2), 0.87 (t, 9H; CH_3).

3,4,5-Tris(*n*-dodecan-1-yloxy)benzoic Acids (2). After the addition of KOH (1.63 g, 30 mmol) into the solution of methyl

3,4,5-tridodecoxybenzoate (10 g, 15 mmol) in ethanol (200 mL), the resulting mixture was refluxed for 4 h. After cooling of the mixture to room temperature, 1 L of deionized water was added. The resulting mixture was acidified until pH = 1 with HCl. The precipitate was then filtered, washed with deionized water (50 mL \times 2) and diethyl ether (30 mL), and dried under a vacuum to give a white solid (9.5 g, 94%): mp 55–57 °C; ¹H NMR (400 MHz, $CDCl_3$, δ): 7.24 (s, 2H; CH), 3.96–4.01 (m, 6H; CH_2), 1.81–1.77 (m, 6H; CH_2), 1.34–1.46 (m, 6H; CH_2), 1.16–1.39 (m, 48H; CH_2), 0.86 (m, 9H; CH_3); ¹³C NMR (100 MHz, $CDCl_3$, δ): 14.23 (3C; CH_3), 22.90 (3C; CH_2), 26.25 (3C; CH_2), 29.61 (3C; CH_2), 29.77 (3C; CH_2), 29.85 (3C; CH_2), 29.87 (3C; CH_2), 29.91 (3C; CH_2), 30.53 (3C; CH_2), 32.14 (3C; CH_2), 69.35 (2C; COH_2), 73.74 (1C; COH_2), 108.70 (2C; CH), 123.85 (1C; C), 143.33 (1C; CO), 153.04 (2C; CO), 172.34 (C=O); ESI/MS: m/z = 675 [M^+] (calcd. m/z = 674.58).

4,6-(3,4,5-Tris(*n*-dodecan-1-yloxy)benzoyloxy)-2,5-diphenylpyrimidine (3). *N,N*-Dimethylformamide was added to a solution of 3,4,5-tris(*n*-dodecan-1-yloxy)benzoic acids (5 g 7.4 mmol) and dried THF (30 mL). After cooling of the reaction flask with an ice bath, thionyl chloride (0.58 mL, 8.0 mmol) was introduced dropwise. The reaction mixture was stirred for 3 h after the ice bath was removed. After filtration and evaporation, sodium hydride (0.16 g, 6.5 mmol) was added to a solution of 4,6-dihydroxy-2,5-diphenylpyrimidine (0.81 g, 3.1 mmol) in dried THF (50 mL). After stirring for 1 h at room temperature, 3,4,5-tris(*n*-dodecan-1-yloxy)benzoic chloride was added. The solution was refluxed for 12 h. After filtration and evaporation, the product was purified by silica (SiO_2) column chromatography eluting with a mixture of ethyl acetate and hexane (4:1, v/v) to give a light yellow powder (2.7 g, 55%): mp 39–43 °C; ¹H NMR (400 MHz, $DMSO-d_6$, δ): 8.47 (d, 4H; CH), 7.47 (m, 4H; CH), 7.25–7.32 (m, 2H; CH), 7.22 (s, 4H; CH), 3.95–3.98 (m, 12H; CH_2), 1.79–1.82 (m, 12H; CH_2), 1.39–1.49 (m, 12H; CH_2), 1.27 (m, 96H; CH_2), 0.89 (m, 18H; CH_3); ¹³C NMR (100 MHz, $CDCl_3$, δ): 14.25 (3C; CH_3), 22.84 (3C; CH_2), 26.23 (3C; CH_2), 29.52 (3C; CH_2), 29.55 (3C; CH_2), 29.71 (3C; CH_2), 29.79 (3C; CH_2), 29.85 (3C; CH_2), 30.49 (3C; CH_2), 32.08 (3C; CH_2), 69.39 (2C; COH_2), 73.74 (1C; COH_2), 108.97 (4C; CH), 117.49 (1C; C), 122.80 (2C; C), 128.51 (2C; C), 128.69 (2C; C), 128.89 (2C; C), 129.49 (2C; C), 129.65 (2C; C), 131.66 (1C; C), 133.21 (1C; C), 136.12 (2C; C–O), 143.63 (4C; C–O), 153.02 (1C; N–C=N), 163.38 (1C; C=O), 165.49 (2C; C=N); MALDI-ToF: m/z = 1600.69 [$M + Na^+$] (calcd. m/z = 1600.23).

RESULTS AND DISCUSSION

Programmed Butterfly-Shaped Diphenylpyrimidine Molecule. A butterfly-shaped DPP molecule having two tridodecyl benzoate tails (6C12) at both sides of the diphenylpyrimidine moiety is specifically designed and synthesized via three-step reactions, as shown in Scheme 1. Especially, an esterification reaction in the presence of 1,3-dicyclohexyl carbodiimide (DCC) and 4-dimethylaminopyridine (DMAP) is conducted. The butterfly-shaped DPP molecule is abbreviated as DPP-6C12. Here, 6 stands for the number of alkyl tails with 12 carbons in each tail. The synthesized DPP-6C12 compound was extensively purified by column chromatography several times. The chemical structure and purity were confirmed by MALDI-ToF mass spectroscopy (Figure 1) in addition to NMR. The molecular weight of DPP-6C12 was determined to be 1578.4 g/mol.

Thermodynamic Transitions of DPP-6C12. As represented in Figure 2, the DSC experiment is first conducted to obtain information on the quantitative thermodynamic properties of the DPP-6C12. At different cooling rates from 0.5 to 40 °C/min in the investigated temperature range, DSC thermograms exhibit only a single exothermic transition around –10 °C. Upon increasing the cooling rate, the onset temperature shifts to lower temperatures and the heat (ΔH) release at the

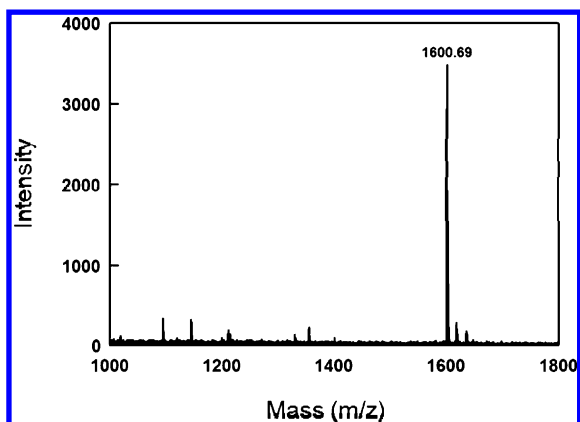


Figure 1. MALDI-ToF spectrum of DPP-6C12 molecule.

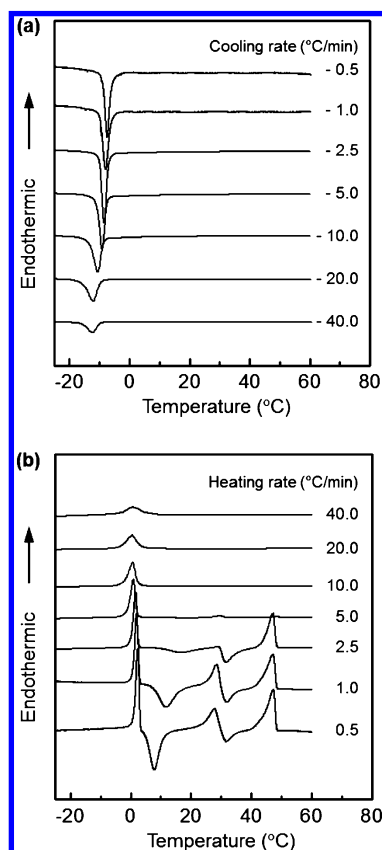


Figure 2. Sets of DSC cooling (a) and subsequent heating (b) thermodiagrams for DPP-6C12 at scanning rates ranging from 0.5 to 40 °C/min.

transition is reduced. At the 0.5 °C/min cooling rate, the onset temperature of the exothermic transition and corresponding heat is -6.5 °C and -27.3 J/g (-43 kJ/mol), respectively, which are reduced to -14.49 °C and -14.8 J/g (-23 kJ/mol) at 40 °C/min. From the linear dependence on the cooling rate,^{27–39} the onset transition temperature and heat at the equilibrium state are estimated to be -5.5 °C and -27.5 J/g (-43.4 kJ/mol), respectively. The dependence of the transition temperature on the cooling rate often means that the exothermic transition is related with a crystallization process.^{34,36} Even though the thermodynamic properties obtained from the subsequent heating process above 10 °C/min are consistent with those from the corresponding cooling

processes, thermal transition behaviors are quite complicated below the 10 °C/min heating rate, as shown in Figure 2b. During the subsequent heating at 0.5 °C/min, an endothermic thermal transition is first occurred at -1.8 °C with 43 kJ/mol, whose transition corresponds to the exothermic transition detected during the previous cooling process. At different heating rates from 0.5 to 2.5 °C/min, two endothermic transitions and two exothermic transitions are observed. When the heating rate is increased from 0.5 to 2.5 °C/min, the onset temperature of the first exothermic peak shift to higher temperatures and the heat (ΔH) release is reduced.

The peculiar thermal transition behaviors depending on the rate of heating process could be originated from the metastable phase transitions, which are related with phase transformation kinetics.^{13,29,30,40} In order to prove that there is a transformation from the metastable/unstable phases to the stable phases, specifically designed experiments were conducted. The DPP-6C12 sample is cooled to 7 °C (Figure 3a) or 30 °C

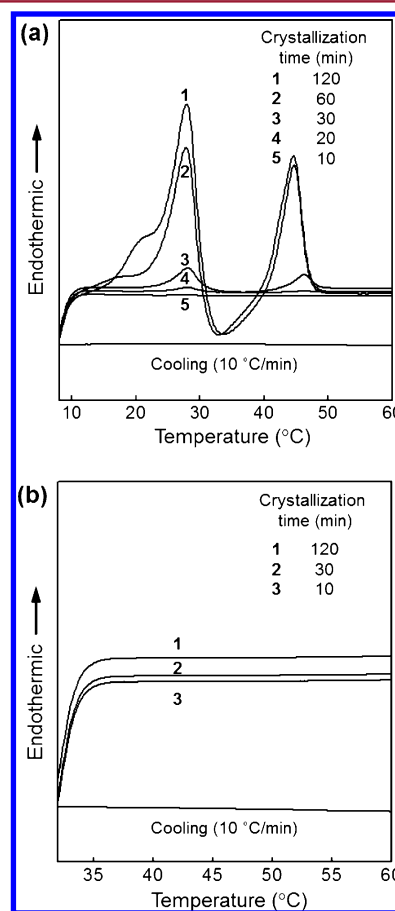


Figure 3. Sets of DSC thermodiagram by cooling DPP-6C12 from the I state at a rate of 10 °C/min to 7 °C (a) and 30 °C which are the onset temperature of the first and second exothermic peaks during heating, and then staying there for different time periods before the sample was heated at 10 °C/min to above the melting temperature.

(Figure 3b) at 10 °C/min and isothermally annealed for the different periods of time. As shown in Figure 3a, the annealed DPP-6C12 samples at 7 °C for the different periods of time are heated to above the highest endothermic transition temperature (45 °C) at 10 °C/min. The heating diagram of the annealed DPP-6C12 samples at 28 °C for 10 min does not exhibit any thermal transition (Figure 3a), which is identical to the heating

diagrams obtained by scanning above 10 °C/min (Figure 2b). After 20 min of annealing, two endothermic transition peaks at 28 and 46 °C start to emerge, and their heats of transitions are saturated after the 120 min annealing.

Note that, in the DPP-6C12 samples annealed for more than 60 min, an exothermic thermal transition appears right after the endothermic transition at 45 °C. To know whether there is a phase transformation from the metastable/unstable phases to the stable phases at 45 °C, similar isothermal annealing experiments are conducted and their results are shown in Figure 3b. In the experimental time scale, any thermal transition is not detected. This indicates that the stable phase between 30 and 40 °C is only formed by a slow heating from the preordered phase observed between 40 and 50 °C, and the formation of the stable phase directly from the I state is forbidden because the nucleation barrier from the I state to the stable crystalline phase is too high to be overcome via thermal annealing in the experimental time scales.

Monotropic Phase Evolutions of DPP-6C12. The 1D WAXD experiments are conducted at different temperatures to identify the corresponding structural evolutions of DPP-6C12. Figure 4 shows a set of 1D WAXD powder patterns of DPP-

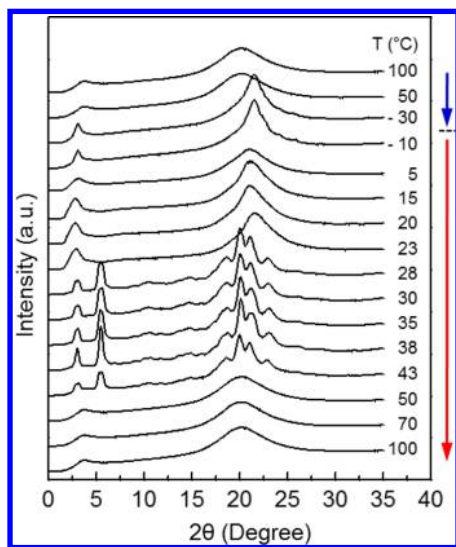


Figure 4. A set of 1D WAXD powder patterns of DPP-6C12 during cooling and subsequent heating at a rate of 1.0 °C/min at different temperatures between −30 and 100 °C.

6C12 at different temperatures between −30 and 100 °C during cooling and subsequent heating at the rate of 1 °C/min. In this figure, structures can be identified on two different length scales. One is on the nanometer scale between $2\theta = 1.5^\circ$ and 7° , and the other is on the subnanometer scale above $2\theta = 7^\circ$.

Upon cooling DPP-6C12, it is obvious that phase transition takes place when the temperature reaches -8°C , which agrees well with crystallization behavior observed in DSC (Figure 2). Above -8°C , the DPP-6C12 molecules are in the I state, exhibiting only two amorphous halos at $2\theta = 3.6^\circ$ ($d = 2.45$ nm) and $2\theta = 20.2^\circ$ ($d = 0.44$ nm), which correspond to the average periodicity of electron density fluctuations between the nanophase separated DPP cores and alkyl tails and to the average distance among the amorphous alkyl chains, respectively. Below -8°C , the amorphous halos at $2\theta = 3.6^\circ$ and $2\theta = 20.2^\circ$ in the I phase are suddenly shifted to $2\theta = 3.06^\circ$

and $2\theta = 21.53^\circ$, respectively, and the half width of these scatterings are dramatically decreased. However, the correlation lengths of these scatterings are still in the quasi-long-range order. Additionally, weak diffraction peaks are observed at $2\theta = 22.36^\circ$, $2\theta = 24.29^\circ$, and $2\theta = 25.64^\circ$. These weak diffractions should relate to the molecular packing of alkyl tails.

To confirm this speculation, the solid-state ^{13}C NMR spectra with CP/MAS/DD (Figure 5a) and Bloch decay (Figures 5b

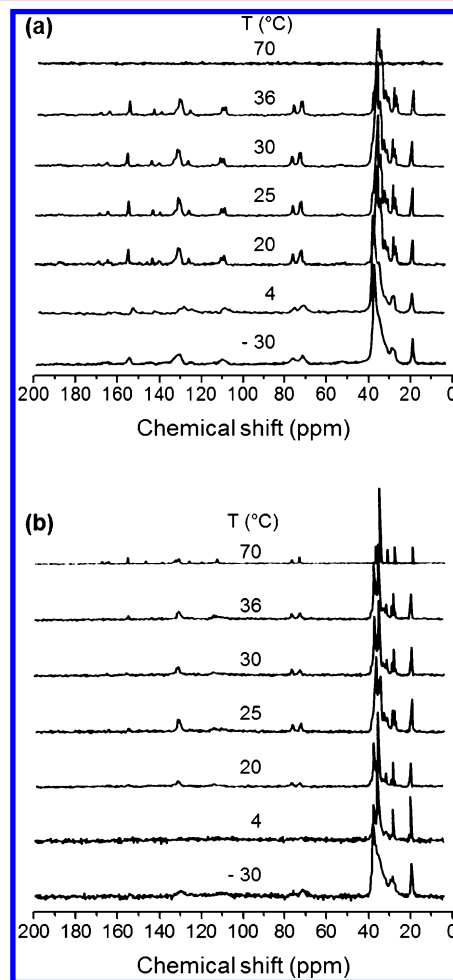


Figure 5. Solid-state ^{13}C NMR spectra of DPP-6C12 during heating from −30 to 70 °C at a rate of 1.0 °C/min: CP/MAS (a) and Bloch decay (b).

and 6) were acquired at different temperatures to selectively investigate the rigid and mobile components, respectively. The solid-state ^{13}C NMR spectra with CP/MAS/DD and Bloch decay below 4°C are not much changed in the chemical shift from 100 to 200 ppm, compared with those of the I state. The chemical shift at 30.0 ppm in the Bloch decay ^{13}C solid-state NMR spectra of DPP-6C12 (Figure 6) is originated from the carbon atoms in the disordered, statistically distributed *trans* and *gauche* conformations. On the other hand, the chemical shift at 32.5 ppm represents the carbon atoms in the long *trans* zigzag segments of the alkyl tails. Below -10°C , more than 70% of CH_2 carbon atoms are in the relatively long *trans* zigzag conformations, while the percentage of *trans* conformations in the I phase is below 10%. This solid-state ^{13}C NMR results combined with those of 1D WAXD indicate that the nanophase separated DPP mesogens are in the solidified and quasi-long-

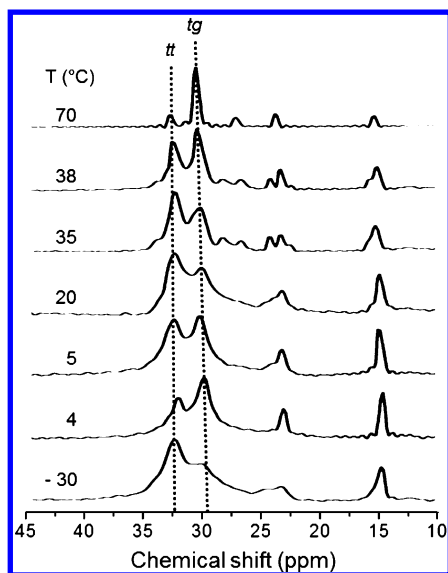


Figure 6. Solid-state ^{13}C NMR spectra of DPP-6C12 during heating from -30 to 70 $^{\circ}\text{C}$ at a rate of 1.0 $^{\circ}\text{C}/\text{min}$: Bloch decay spectra between 10 and 45 ppm.

range ordered state below -10 $^{\circ}\text{C}$, but the individual carbons in DPP mesogens are quite mobile compared with those of the well-ordered phases.

After subsequent heating of the DPP-6C12 sample from -30 to 5 $^{\circ}\text{C}$, the amorphous halos at $2\theta = 3.06^{\circ}$ ($d = 2.88$ nm) and $2\theta = 21.53^{\circ}$ ($d = 0.41$ nm) shifted to $2\theta = 3.11^{\circ}$ ($d = 2.85$ nm) and $2\theta = 21.02^{\circ}$ ($d = 0.42$ nm) (Figure 4), respectively, and the half width of these scatterings suddenly increased. Additionally, weak diffractions observed at $2\theta = 22.36^{\circ}$, $2\theta = 24.29^{\circ}$ and $2\theta = 25.64^{\circ}$ disappeared. Therefore, the diffraction pattern at 5 $^{\circ}\text{C}$ is very similar to that of the I state. This result indicates that the endothermic transition at 2 $^{\circ}\text{C}$ is originated to the ordered alkyl chain melting. Again, this explanation can be supported by solid-state ^{13}C NMR spectra with CP/MAS/DD (Figure 5a) and Bloch decay (Figures 5b and 6) at 4 $^{\circ}\text{C}$. The 70% of CH_2 carbon atoms in the relatively long *trans* zigzag conformations is suddenly decreased to 30% at 4 $^{\circ}\text{C}$. Additionally, the carbon atoms in DPP mesogens are increased by melting alkyl tails of DPP-6C12. Since the thermal transition below 5 $^{\circ}\text{C}$ is due to the alkyl tail crystallization and melting of DPP-6C12, this phase is identified as the plastic crystal (PK) phase.

By annealing the DPP-6C12 sample between 5 and 25 $^{\circ}\text{C}$, the metastable I state is gradually transformed to a stable mesophase. As shown in Figure 4, the amorphous halos at $2\theta = 3.11^{\circ}$ and $2\theta = 21.02^{\circ}$ at 5 $^{\circ}\text{C}$ gradually shifted to $2\theta = 2.83^{\circ}$ ($d = 3.12$ nm) and $2\theta = 21.5^{\circ}$ ($d = 0.43$ nm), respectively, and the half width of these scatterings decreased. This gradual phase transformation from the metastable I state to a stable mesophase between 5 and 25 $^{\circ}\text{C}$ was also detected by solid-state ^{13}C NMR spectra. As represented in solid-state ^{13}C NMR spectra with CP/MAS/DD (Figure 5a) and Bloch decay (Figures 5b and 6), the mobility of carbon atoms in DPP mesogens considerably increased and the percentage of the CH_2 long *trans* zigzag conformations again increased up to 60%. Note that this percentage is a little bit lower than that of the PK phase. On the basis of the experimental results of 1D WAXD and solid-state ^{13}C NMR, it is concluded that this phase is a traditional columnar LC phase (Φ) which is originated by the nanophase separation between aromatic DPP cores and

flexible alkyl tails as well as by the molecular stacking among aromatic DPP cores. This molecular stacking among aromatic DPP cores increases the amount of CH_2 long *trans* zigzag conformations, but the alkyl tails are not in the 3D crystalline phase, similar to the traditional mesophases.

After continually increasing temperature up to 40 $^{\circ}\text{C}$ (Figure 2b), an endothermic thermal transition was detected at 28 $^{\circ}\text{C}$ right after the exothermic transition at 32 $^{\circ}\text{C}$. By heating the stable Φ mesophase, the molecular mobility gradually increased, and the thermal fluctuation was enough to overcome the nucleation barrier. This explanation is supported by the structure-sensitive 1D WAXD. As shown in Figure 4, a lot of diffractions are detected not only in the small angle but also in the wide angle regions, which represent a 3D ordered crystalline structure of DPP-6C12. It is worth mentioning that the percentage of the CH_2 long *trans* zigzag conformations is slightly decreased from 60% (Φ mesophase) to 55%, even though the rigidity of aromatic carbons is increased compared with those of the Φ mesophase. This crystalline phase is identified as the K phase. Since the 2D WAXD pattern from a macroscopically oriented sample and selected area electron diffraction from a single crystal are required to identify the detail molecular packing in the K phase, the identification of ordered K phase is under investigation. From the experimental results, it is found that the strong molecular packing among DPP mesogens can distort molecular ordering of alkyl tails. Therefore, it is concluded that the PK phase is due to the alkyl chain crystallization, while the K phase is induced by the strong molecular packing among DPP mesogens. Note that the K phase could not be formed directly from the I state but from the preordered Φ mesophase because the nucleation barrier from the I state to the K phase is too high to be overcome via thermal annealing in experimental time scales. The unique phase transition behaviors of DPP-6C12 should originate from the distorted mesogens which make it difficult to pack by themselves.

Morphological Phase Transition Behaviors of DPP-6C12. The peculiar phase transformation behaviors of DPP-6C12 are further investigated by POM texture changes, which can provide morphological information on the micrometer length scale depending on phase evolutions. Figure 7 shows the POM micrographs of DPP-6C12 samples at -30 , 20 , and 35 $^{\circ}\text{C}$ after cooling from the I state at rate of 1 $^{\circ}\text{C}/\text{min}$. No birefringence is detected in the PK phase. Only alkyl chains of DPP-6C12 compound are crystallized in the PK phase, a fact clearly identified based on the 1D WAXD combined with DSC and solid-state ^{13}C NMR. However, the synergistic organization of alkyl chains is not strong enough to generate detectable birefringences in the POM experiments. By increasing temperature at 1 $^{\circ}\text{C}/\text{min}$, a POM texture of the stable Φ mesophase was obtained between 7 and 25 $^{\circ}\text{C}$, as shown in Figure 7b. Strong birefringence starts to emerge against the dark background. As mentioned above, DPP mesogens in the Φ mesophase are stacked each other, while the alkyl chains are more or less in a molten state. From this result, it is realized that the major cause of strong birefringence in the Φ mesophase is from the strong molecular packing among DPP mesogens of DPP-6C12 compound rather than the organization of alkyl chains. After continuously increasing temperature above 30 $^{\circ}\text{C}$, the K crystalline phase was obtained, and its POM texture is represented in Figure 7c. The strong birefringence in the K phase should be mainly originated

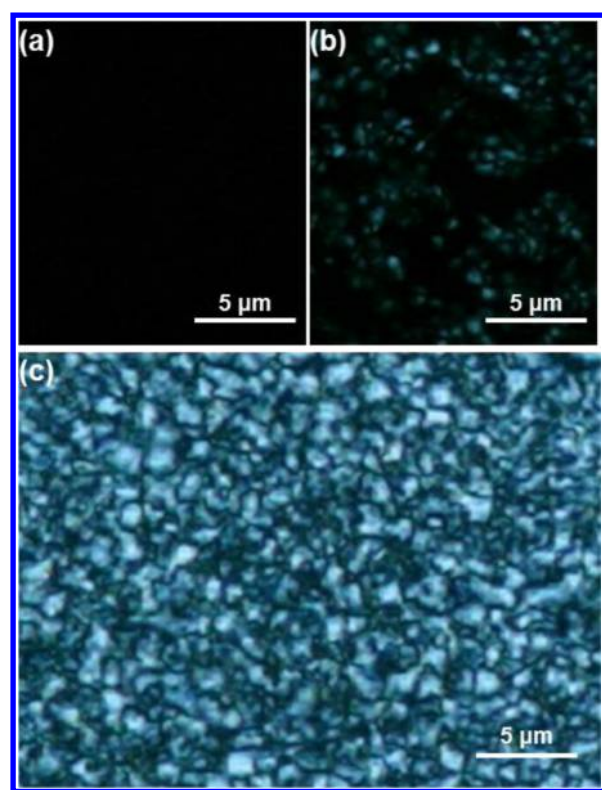


Figure 7. POM image of DPP-6C12 at different temperatures during heating from -30 to 35 °C at a rate of 1.0 °C/min: -30 °C (a), 20 °C (b), and 35 °C (c).

from the DPP mesogens, which are closely packed in the 3D long-range ordered crystalline lattice.

Monotropic Phase Transition Diagram of DPP-6C12.

To understand the peculiar monotropic phase transition behaviors of DPP-6C12,^{13,29,30,40} the free energy versus temperature at constant pressure is schematically illustrated in Figure 8. As represented as blue arrows in Figure 8, upon

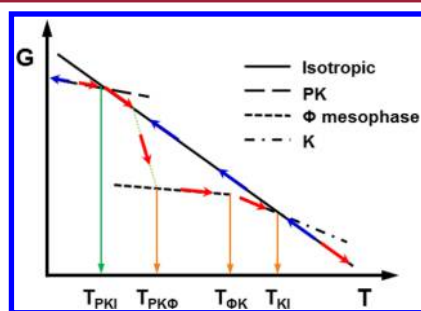


Figure 8. Illustration of the free energy versus temperature at constant pressure for DPP-6C12. Here, blue and red arrows represent the cooling and heating tracks.

cooling DPP-6C12, the I phase transfers to the PK phase which possesses the lowest free energy phase below T_{PKI} . During the cooling process from the I state, any phase transformation does not occur above T_{PKI} . This means that the nucleation barriers to form any mesophases or crystalline phases are too high so that no phase transitions are observed even at 0.5 °C/min cooling. With subsequently heating DPP-6C12 at the rate of 10 °C/min, only T_{PKI} transition is detected by melting alkyl chain crystals, as show in Figure 2. However, with slowly heating

DPP-6C12 at the rate of 0.5 °C/min (represented as red arrows), the stable Φ mesophase gradually emerged above $T_{PK\Phi}$ and below $T_{\Phi K}$. This means that, between $T_{PK\Phi}$ and below $T_{\Phi K}$, the superheated I state is in a metastable state, and the stable Φ mesophase can be obtained by providing enough time for DPP-6C12 to find a pathway into the stable Φ mesophase. As represented before, this explanation is further confirmed by the isothermal annealing (Figure 3a). When this stable Φ mesophase is heated up to $T_{\Phi K}$, the K crystalline phase is formed. In this stable K phase, both DPP mesogens and alkyl tails of DPP-6C12 are closely packed into the 3D long-range ordered lattice. From the isothermal annealing experiments (Figure 3b), it is realized that the stable K phase is only formed by a slow heating from the preordered Φ mesophase, and the formation of the K phase directly from the I state is forbidden because the nucleation barrier from the I state to the K phase is too high to be overcome via thermal annealing. Finally, the K crystal is melted at T_{KI} and goes back to the I state.

CONCLUSIONS

A butterfly-shaped diphenylpyrimidine molecule (abbreviated as DPP-6C12) was newly designed and successfully synthesized. By the combination of thermal, scattering, spectroscopic, and microscopic experiments, it was realized that DPP-6C12 formed a plastic crystal phase (PK), a crystal phase (K), and a liquid crystal phase (Φ). The stable Φ mesophase was formed either by a subsequent slow heating above the PK phase or by an isothermal annealing between T_{Φ} and T_K . The stable K phase was only formed by a slow heating from the preordered Φ mesophase, and the formation of the K phase directly from the isotropic state (I) is forbidden because the nucleation barrier from the I state to the K phase is too high to be overcome via thermal annealing in experimental time scales. This peculiar monotropic phase transition behaviors of DPP-6C12 should be originated from the nonplanarity of DPP-6C12 aromatic mesogen. From the 1D WAXD results combined with those of DSC and solid-state ^{13}C NMR, it was realized that the driving forces of the PK phase formation are the nanophase separation between alkyl tails and rigid aromatic cores as well as the crystallization of alkyl tails. In the PK phase, aromatic cores did not participate in the crystallization and remained as a disordered state. On the other hand, the aromatic cores in the Φ mesophase were ordered to form the self-assembled nanocolumns by π - π interactions, but the alkyl tails were in a molten state.

ASSOCIATED CONTENT

Supporting Information

General experimental procedures and operating methods of equipment. This material is available free of charge via the Internet at <http://pubs.acs.org>.

AUTHOR INFORMATION

Corresponding Authors

*(K.-U.J.) E-mail: kujeong@jbnu.ac.kr.

*(S.-H.H.) E-mail: bach@dankook.ac.kr.

Notes

The authors declare no competing financial interest.

ACKNOWLEDGMENTS

This work has been supported by the Basic Science Research Program (2013R1A1A2007238), KIST institutional program

(2Z04320), and BK21 Plus Program, Korea. D.Y.K. appreciates the support from Global Ph.D. Fellowship Program.

REFERENCES

- (1) Oxtoby, D. W.; Shen, Y. C. *J. Phys.: Condens. Matter* **1996**, *8*, 9657.
- (2) Andrews, B. M.; Gray, G. W.; Bradshaw, M. J. *Mol. Cryst. Liq. Cryst.* **1985**, *123*, 257.
- (3) Bolhuis, P. G.; Frenkel, D.; Mau, S.-C.; Huse, D. A. *Nature* **1997**, *388*, 235.
- (4) Buffat, P. h.; Borel, J.-P. *Phys. Rev. A* **1976**, *13*, 2287.
- (5) Carr, N.; Gray, G. W. *Mol. Cryst. Liq. Cryst.* **1985**, *124*, 27.
- (6) Dick, K.; Dhanasekaran, T.; Zhang, Z.; Meisel, D. *J. Am. Chem. Soc.* **2001**, *124*, 2312.
- (7) Jing, A. J.; Taikum, O.; Li, C. Y.; Harris, F. W.; Cheng, S. Z. D. *Polymer* **2002**, *43*, 3431.
- (8) Moroni, D.; Ten Wolde, P. R.; Bolhuis, P. G. *Phys. Rev. Lett.* **2005**, *94*, 235703.
- (9) Rastogi, S.; Newman, M.; Keller, A. *Nature* **1991**, *353*, 55.
- (10) Evans, R. M.; Poon, W. C. K. *Phys. Rev. E* **1997**, *56*, 5748.
- (11) van Ruth, N. J. L.; Rastogi, S. *Macromolecules* **2004**, *37*, 8191.
- (12) Tang, B. Y.; Jing, A. J.; Li, C. Y.; Shen, Z.; Wang, H.; Harris, F. W.; Cheng, S. Z. D. *Cryst. Growth Des.* **2003**, *3*, 375.
- (13) Cheng, S. Z. D. *Phase Transitions in Polymers: The Role of Metastable States*; Elsevier Science: Akron, 2008; pp 61–72.
- (14) Segura, J. L.; Martín, N. *Angew. Chem., Int. Ed.* **2001**, *40*, 1372.
- (15) Rahman, M. L.; Tschierske, C.; Yusoff, M.; Silong, S. *Tetrahedron Lett.* **2005**, *46*, 2303.
- (16) Schmidt-Mende, L.; Fechtenkötter, A.; Müllen, K.; Moons, E.; Friend, R. H.; MacKenzie, J. D. *Science* **2001**, *293*, 1119.
- (17) Laschat, S.; Baro, A.; Steinke, N.; Giesselmann, F.; Hägele, C.; Scalia, G.; Judele, R.; Kapatsina, E.; Sauer, S.; Schreivogel, A.; Tosoni, M. *Angew. Chem., Int. Ed.* **2007**, *46*, 4832.
- (18) Tang, C. W. *Appl. Phys. Lett.* **1986**, *48*, 183.
- (19) Ungar, G.; Feijoo, J. L.; Percec, V.; Yourd, R. *Macromolecules* **1991**, *24*, 953.
- (20) Tang, C. W.; VanSlyke, S. A. *Appl. Phys. Lett.* **1987**, *51*, 913.
- (21) Burroughes, J. H.; Bradley, D. D. D.; Brown, A. R.; Marks, R. N.; Mackay, K.; Friend, R. H.; Burns, P. L.; Holmes, A. B. *Nature* **1990**, *347*, 539.
- (22) Shirota, Y.; Kageyama, H. *Chem. Rev.* **2007**, *107*, 953.
- (23) Yandrasits, A.; Cheng, S. Z. D.; Zhang, A.; Cheng, J.; Wunderlich, B.; Percec, V. *Macromolecules* **1992**, *25*, 2112.
- (24) Mosquera, A.; Riveiros, R.; Sestelo, J. P.; Sarandeses, L. A. *Org. Lett.* **2008**, *10*, 3745.
- (25) Ivanova, E. V.; Balashev, K. P. *Opt. Spectrosc.* **2010**, *108*, 574.
- (26) Itami, K.; Yamazaki, D.; Yoshida, J.-i. *J. Am. Chem. Soc.* **2004**, *126*, 15396.
- (27) Sergeev, S.; Pisulab, W.; Geerts, Y. H. *Chem. Soc. Rev.* **2007**, *36*, 1902.
- (28) Kastler, M.; Pisula, W.; Laquai, F.; Kumar, A.; Davies, R. J.; Balushev, S.; Garcia-Gutiérrez, M.-C.; Wasserfallen, D.; Butt, H.-J.; Riekel, C.; Wegner, G.; Müllen, K. *Adv. Mater.* **2006**, *18*, 2255.
- (29) Pardey, R.; Zhang, A.; Gabori, P. A.; Harris, F. W.; Cheng, S. Z. D.; Adduci, J.; Facinelli, J. V.; Lenz, R. W. *Macromolecules* **1992**, *25*, 5060.
- (30) Pardey, R.; Shen, D.; Gabori, P. A.; Harris, F. W.; Cheng, S. Z. D.; Adduci, J.; V. Facinelli, J.; Lenz, R. W. *Macromolecules* **1993**, *26*, 3687.
- (31) Yoon, Y.; Zhang, A.; Ho, R.-M.; Cheng, S. Z. D.; Percec, V.; Chu, P. *Macromolecules* **1996**, *29*, 294.
- (32) Yoon, Y.; Ho, R.-M.; Moon, B.; Kim, D.; McCreight, K. W.; Li, F.; Harris, F. W.; Cheng, S. Z. D.; Percec, V.; Chu, P. *Macromolecules* **1996**, *29*, 3421.
- (33) Zheng, R.-Q.; Chen, E.-Q.; Cheng, S. Z. D.; Xie, F.; Yan, D.; He, T.; Percec, V.; Chu, P.; Ungar, G. *Macromolecules* **1999**, *32*, 3574.
- (34) Zheng, R.-Q.; Chen, E.-Q.; Cheng, S. Z. D.; Xie, F.; Yan, D.; He, T.; Percec, V.; Chu, P.; Ungar, G. *Macromolecules* **1999**, *32*, 6981.
- (35) Jeong, K.-U.; Jin, S.; Ge, J. J.; Knapp, B. S.; Graham, M. J.; Ruan, J.; Guo, M.; Xiong, H.; Harris, F. W.; Cheng, S. Z. D. *Chem. Mater.* **2005**, *17*, 2852.
- (36) Jeong, K.-U.; Knapp, B. S.; Ge, J. J.; Jin, S.; Graham, M. J.; Xiong, H.; Harris, F. W.; Cheng, S. Z. D. *Macromolecules* **2005**, *38*, 8333.
- (37) Jeong, K.-U.; Knapp, B. S.; Ge, J. J.; Graham, M. J.; Tu, Y.; Leng, S.; Xiong, H.; Harris, F. W.; Cheng, S. Z. D. *Polymer* **2006**, *47*, 3351.
- (38) Jeong, K.-U.; Yang, D. K.; Graham, M. J.; Tu, Y.; Kuo, S. W.; Knapp, B. S.; Harris, F. W.; Cheng, S. Z. D. *Adv. Mater.* **2006**, *18*, 3229.
- (39) Yang, D.-K.; Jeong, K.-U.; Cheng, S. Z. D. *J. Phys. Chem. B* **2008**, *112*, 1358.
- (40) Pardey, R.; Wu, S. S.; Chen, J. H.; Harris, F. W.; Cheng, S. Z. D.; Adduci, J.; Facinelli, J. V.; Lenz, R. W. *Macromolecules* **1994**, *27*, 5794.